AN INTEGRATED APPROACH FOR STRUCTURAL HEALTH MONITORING OF CONCRETE STRUCTURES BASED ON ELECTROMECHANICAL ADMITTANCE AND GUIDED WAVES

CONFERENCE PAPER · JUNE 2013

CITATIONS
2

READS
43

6 AUTHORS, INCLUDING:

Costas Providakis
Technical University of Crete
64 PUBLICATIONS **345** CITATIONS
SEE PROFILE

Kalliope Stefanaki
Technical University of Crete
10 PUBLICATIONS **7** CITATIONS
SEE PROFILE

M.E. Voutetaki
Technical University of Crete
15 PUBLICATIONS **11** CITATIONS
SEE PROFILE

Maria E. Stavroulaki
Technical University of Crete
21 PUBLICATIONS **35** CITATIONS
SEE PROFILE

6th ECCOMAS Conference on Smart Structures and Materials
SMART2013
Politecnico di Torino, 24-26 June 2013
C. Providakis, K. Stefanaki, M. Voutetaki, J. Tsompanakis, M. Stavroulaki and J. Agadakos
www.smart2013.com

AN INTEGRATED APPROACH FOR STRUCTURAL HEALTH MONITORING OF CONCRETE STRUCTURES BASED ON ELECTROMECHANICAL ADMITTANCE AND GUIDED WAVES

C. Providakis, K. Stefanaki, M. Voutetaki, J. Tsompanakis, M. Stavroulaki and J. Agadakos

Technical University of Crete
Department of Applied Sciences
Applied Mechanics Lab, University Campus
GR-73100, Chania, Greece
e-mail: cpprov@mred.tuc.gr, web page: http://users.isc.tuc.gr/~kprovidakis

Key words: Concrete structures, Electro-mechanical admittance, Guided waves, PZT, Damage detection, FFT spectrum.

Summary. *An integrated monitoring approach for near and far-field damage detection in concrete structures based on simultaneous use of electromechanical admittance and guided wave propagation is presented in this work. The proposed sensing system uses arrays of PZT patches bonded on the surfaces of concrete structures which are serving as multi-mode sensors/actuators. This innovative technique takes advantage of two PZT basic capabilities: a) to serve as near-field damage detection sensors using the high-frequency electromechanical (E/M) admittance monitoring technique and b) to serve as far-field damage detection sensors using guided wave propagation monitoring technique. In the guided wave propagation, one PZT patch acts as actuator and launches an elastic wave through the structure, which then can be measured by another PZT patch which in the same time serves as admittance sensor. The integration approach of both two methodologies is then straightforward because the same piezoelectric patch can be used for both methods. This integration approach is experimentally validated in this work by inspecting the sensing capabilities of custom-made "multi-mode" sensing system for damage detection of concrete structures.*

1 INTRODUCTION

Many traditional visual or localized experimental structural health monitoring (SHM) and damage detection methods have been proposed in the past and have been used in a variety of concrete structures such as C-scan, X-rays, radar techniques, etc [1-4]. However, all these experimental techniques require bulky equipments and they are extremely time-consuming and most importantly they request that the vicinity of the damage is known a priori while the portion of the structure to be inspected is readily accessible. As concrete structures become

larger and more complex those techniques become non-feasible and not suitable for in-service infrastructures.

One of the most promising active sensing approaches which utilizes piezoelectric transducers as actuators/sensors, the electromechanical admittance, or its inverse impedance, the so-called EMA technique, has received growing attention in recent years for in-situ health monitoring due to its distinct advantages [5-6]. EMA response is derived from the dynamic interaction between piezoelectric transducers (PZT) and the host structure. EMA is typically applied using an electrical impedance analyzer which scans a predefined frequency range in the order of tens to hundreds of kHz. The main advantage of EMA technique is its capability to detect local damages, even in complex structures.

Guided wave (GW) technique uses stress waves that propagate in rods, rails, beams and plates [13-17]. The boundaries of the host structure 'guide' those stress waves along the length of the structure, utilizing them for detecting structural damages. It presents an essential advantage over many other identification techniques allowing long distance wave propagation with little attenuation. When guided waves pass through a damaged region then scattering, reflection, and finally mode conversion takes place. By investigating the characteristics of the reflection as well as the transmitted waves, detailed information on the damage can be obtained.

The simultaneous use of the two above mentioned techniques for improved damage identification has been proposed in previous works [7-9] but the applicability of these techniques to concrete structures has not yet been fully tested or demonstrated. Furthermore, considering the previous integrated methodologies, the work presented herein is quite different, since they performed monitoring by using EMA and guided wave procedures sequentially rather than simultaneously.

As the same type of transducers can be utilized for either technique, we proposed an integrated multi-mode sensing system that detects and investigates the changes in the admittance spectrum of a PZT transducer in the range of a predefined frequency band as generated by a second PZT patch acting as a guided wave transmitter. The main feature of the present work is that incorporating synchronous admittance-based and guided wave propagation measurements retains the benefits of both techniques allowing effective near-field damage detection and in the same time large area's sensing capabilities.

To validate the proposed integrated damage identification technique, a concrete beam specimen is designed and fabricated. Results obtained from measurement data using a custom made impedance measuring circuit are discussed and presented.

2 ELECTRO-MECHANICAL ADMITTANCE (EMA) METHOD

The EMA technique uses piezoelectric materials, such as Lead Zirconate Titanate (PZT), which exhibits the characteristic feature to generate surface charge in response to an applied mechanical stress and conversely, undergo mechanical deformation in response to an applied electric field.

Consider a structural component with a PZT patch bonded on it. The related physical model is shown in Fig. 1 for a square PZT patch of length $2\ell_{PZT}$ and thickness h_{PZT}.

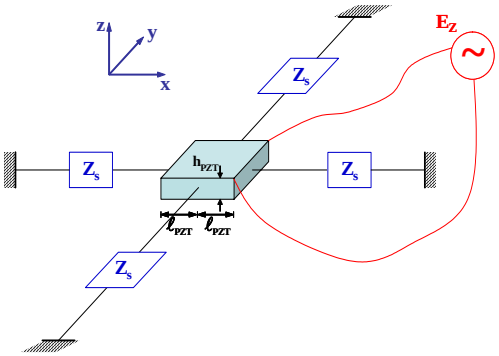

Figure 1: Interaction model of PZT and concrete structure.

The proposed damage detection approach consists of two applied in the z-direction, producing an electric field $E= E_0e^{j\omega t}$, an in-plane vibration is induced in both x and y directions. Liang et al[10] first modeled the 1D PZT-structure electro mechanical interaction, while Bhalla & Soh [11] extended this approach to 2D structures by using the concept of effective impedance.
The constitutive equations of the PZT patch are:

$$S_X = \frac{1}{\bar{E}_{PZT}}\left(T_X - \nu_{PZT} T_Y\right) + d_{31}E \tag{1}$$

$$S_Y = \frac{1}{\bar{E}_{PZT}}\left(T_Y - \nu_{PZT} T_X\right) + d_{32}E \tag{2}$$

$$D = \bar{\varepsilon}_{33}E + d_{31}T_X + d_{32}T_Y \tag{3}$$

Where, $i=\sqrt{(-1)}$, S_X and S_Y are strains, T_X and T_Y are stresses, $\bar{E}_{PZT} = E_{PZT}(1 + ni)$ is the elastic modulus at zero electric field, n is the mechanical loss factor, ν_{PZT} is the Poison's ratio, d_{31} and d_{32} are the piezoelectric constants in the x and y directions, respectively, $\bar{\varepsilon}_{33}^T = \varepsilon_{33}^T(1 - \delta i)$ is the dielectric constant at zero stress, D is the electric displacement and δ the dielectric loss factor. If the PZT material is isotropic on the x-y plane, which results in $d_{31} = d_{32}$, the electric displacement in equation (3) can be rewritten as:

$$\rho_{PZT}\ddot{u} = \frac{\bar{E}_{PZT}}{1 - \nu_{PZT}^2}u'' \tag{4}$$

$$\rho_{PZT}\ddot{v} = \frac{\bar{E}_{PZT}}{1-\nu_{PZT}^2} v'' \tag{5}$$

where $\left(\dot{\ }\right) = \partial(\ )/\partial t$ and ρ_{PZT} is the density of the PZT patch. The electric current passing through the PZT patch, can be considered to be given by

$$I = j\omega \int_{-\frac{\ell_{PZT}}{2}}^{\frac{\ell_{PZT}}{2}} \int_{-\frac{\ell_{PZT}}{2}}^{\frac{\ell_{PZT}}{2}} D\,dx\,dy \tag{6}$$

Considering that the electric field is defined by

$$Y(j\omega) = \frac{I(i\omega)}{V(i\omega)} \tag{7}$$

Hence, the admittance can be evaluated by using:

$$Y(j\omega) = \frac{\mathrm{FFT}\{\mathrm{I(t)}\}}{\mathrm{FFT}\{\mathrm{V(t)}\}} \tag{8}$$

3 CONCRETE BEAM SPECIMEN

Experiments are conducted by mounting two PZT patches embedded in a 150X150X750 mm concrete beam specimen in a setup shown in Figure 2. The concrete beam specimen made by a mixing proportion of 1:0.62:2.25:3.83 (Cement: Water: Fine Aggregate: Coarse Aggregate, ratio by mean of cement)

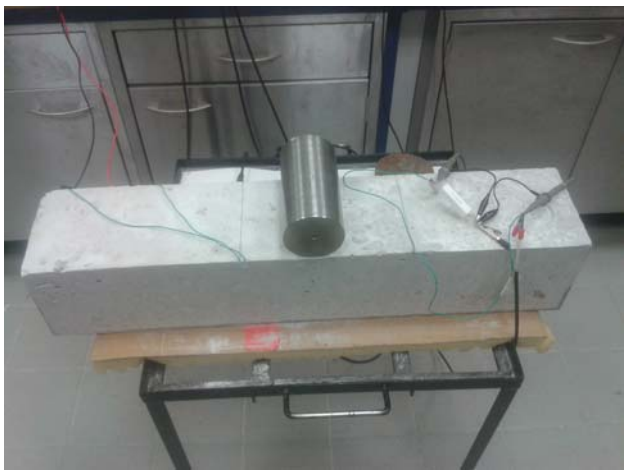

Figure 2: Concrete beam specimen with embedded PZT-based measuring system

Since PZTs are very fragile and can be easily damaged during the casting of the beam specimen, they are embedded into the concrete structure just like its aggregates. Those aggregates have been made using a sandwich method to form a custom-made enclosure. They were formed by joining two pieces of cubic hardened cement mortar blocks with a PZT located between them as shown in Figure 3. The joining was achieved by using an RTV adhesive which is also serving as a shielding against any water penetration which could be dangerous for PZT sensing element that is sensitive to moisture.

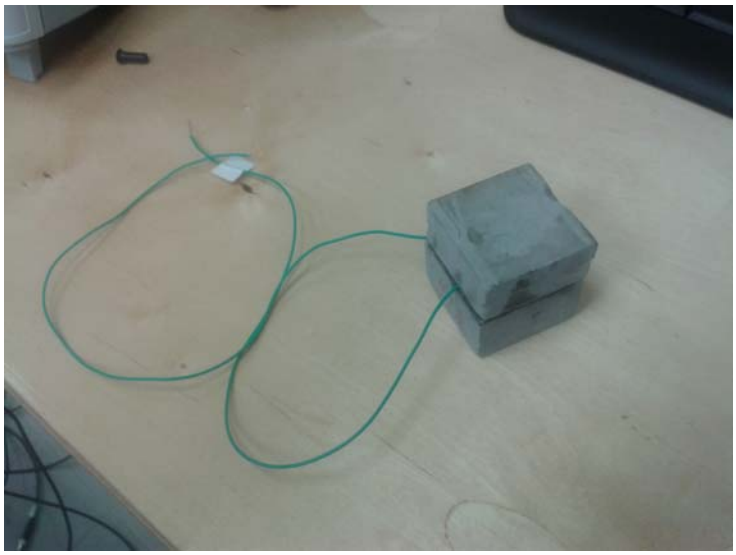

Figure 3: Aggregate-like enclosure for PZT protection

4 CUSTOM-MADE ADMITTANCE MEASURING SYSTEM

For carrying out electrical admittance measurements various commercial admittance analyzer instruments could be used. Among others HP4194A instrument, or QuadTec 7100 LCR meter [12] or Cyber Instruments C60 portable impedance analyzer [13] can be referenced. It is apparent that in order to achieve wide industrial dissemination, any such impedance analyzer instrument cost around a value which should be reduced to a level similar to that of a PZT patch. As a result, an alternative to them, the recently proposed miniaturized chip-based AD-5933 impedance converter network analyzer has been implemented to various applications. Unfortunately, such chip-based solution presents limited capabilities to concrete material-based structure monitoring applications since AD-5933 based measurements are suffering by a narrow frequency range (up to 100 kHz).

In this paper, to measure the unknown admittance (or its inverse impedance) across a PZT's poles we use the I-V methodology [14] by using the measured values of voltage and current. Current is calculated by using the voltage measurement across an accurately known low value

calibrated resistor Ref (say 100Ω). To develop a simple and wide-frequency range admittance measuring circuit, we designed the compact electromechanical admittance measuring system shown in Figure 4.

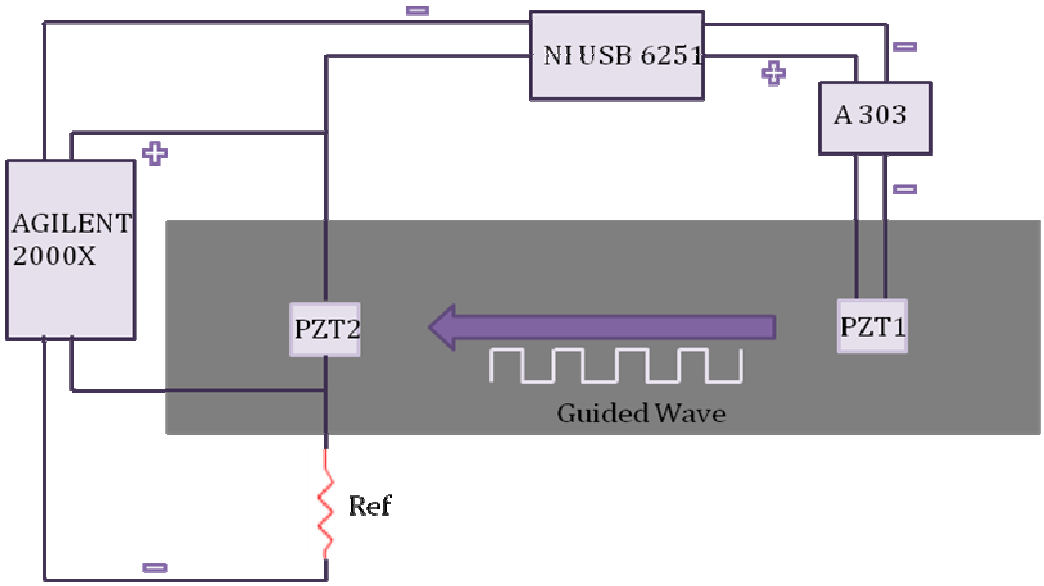

Figure 4: Proof-of-concept demonstration of admittance measuring system

To excite the PZT, a National Instruments USB-6251 high-speed M series multifunction data acquisition (DAQ) module is utilized and optimized for accuracy at fast sampling. This DAQ card contains analog-to-digital (ADC) and digital-to-analog (DAC) converters with 1.25 MSamples/sec speed and 16-bit resolution. The excitation voltage V_{in} is of sinusoid-type having an amplitude of $|V_{in}|$ and a frequency sweeping from F_{start} to F_{end} (say 10kHz to 350kHz). A two-channel Agilent 2000X oscilloscope was used to record simultaneously the time history of voltage $V_{in}(t)$ at one of the output channels of the USB-6251 card and the time history of voltage drop $V_{out}(t)$ on the calibrated resistor Ref. The time history of the current I(t) flowing through the PZT also flows through the resistor Ref. The time history of current I(t) can be calculated as $I(t)=V_{out}(t)/R_{ef}$. Hence, the PZT admittance Y is calculated using an expression of the type:

$$Y(t)=\frac{I(t)}{V(t)}=\frac{V_{out}(t)\cdot\left(\frac{1}{R_{ef}}\right)}{V_{in}(t)-V_{out}(t)} \tag{10}$$

By Fourier transforming the above time domain equation to yield the frequency domain quantities I(iω) and V(iω), the admittance of PZT may be calculated as the transfer function of PZT :

$$Y(i\omega) = \frac{I(i\omega)}{V(i\omega)} \tag{11}$$

Hence, the complex admittance of PZT is

$$Y(t) == \frac{FFT\left(V_{out}(t)\cdot\left(\frac{1}{R_{ef}}\right)\right)}{FFT(V_{in}(t)-V_{out}(t))} = R + iX \tag{12}$$

where, FFT{} designates fast Fourier transform and R is the real part (conductance) and X the imaginary part (susceptance) of the complex admittance. With this approach, the admittance spectrum of an investigated specimen can be acquired even within one wideband excitation signal sweeping.

To achieve such a wide band excitation signal sweeping, a digitally synthesized linear chirp signal is generated (F_{start}=10000 kHz, F_{end}=200000 kHz, F_s=1MHz sample rate, 500 samples) by using Labview SignalExpress program [15] and then transmitted to the admittance measuring circuit by the output channel of USB-6251 card. The actual excitation voltage V_{in} and the response of the PZT, V_{out}, were recorded synchronously by the two-channel BNC input port of Agilent 2000X oscilloscope. The admittance spectrum of the PZT equals FFT of the response signal over the FFT of the excitation signal according to equation (12).

To create the propagating guided wave, a similar to the first one PZT patch is also embedded inside the concrete beam specimen in a distance of 300 mm from the first one. This PZT patch serves as a guided wave actuator by connecting its electrodes to one of the rest output channels of USB-6251 multifunction card. The USB-6251 guided wave output signal was pre-amplified by 20 times using an A-303 AALab piezo-driver [16]. A 10Hz sequence of square guided wave signals, sampled at 1MHz was selected to drive the PZT actuator. The whole experimental arrangement is presented in Figure 5.

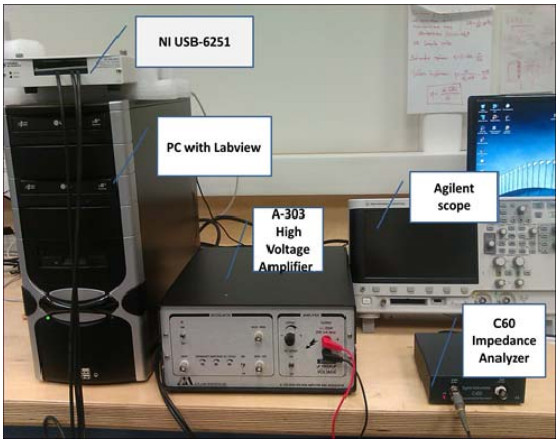

Figure 5: Experimental arrangement

5 EXPERIMENTAL VERIFICATIONS

To experimentally validate the proposed multi-mode integrated monitoring technique we monitor the above described concrete beam specimen. The proposed damage detection approach consists of two basic steps: a) EMA spectra will be acquired for one of the PZT patches (say PZT2) by using the custom made admittance measuring circuit activated by the linear chirp described in equation (13) and b) in the same time, the other PZT patch (say PZT1) is excited by the National Instrument USB-6251 unit running under NI Labview SignalExpress in such a way that in one of its output channels generates a 10kHz sequence of 14V peak-to-peak square guided waves.

$$V_{in} = \sin\left(2\cdot\pi\cdot F_{start}\cdot t + \frac{\left((F_{end}-F_{start})\cdot t\cdot t\right)}{\left(samples\cdot(1/F_S)\right)}\right) \tag{13}$$

Structural damage was artificially introduced by attaching a cylindrical steel mass of 6 Kgr (termed as M1) on the upper surface of a concrete beam in a distance of 100 mm from PZT2 along the line of sight between PZT1 and PZT2 as shown in Figure 6. To further simulate an extended damage area we put an additional steel mass of 2.5 kgr, termed as M2, under the mass of 6.03 kgr giving a total mass of 8.kgr (=6.03 kgr + 2.45 kgr). The approach described here is commonly used in the literature to evaluate and compare SHM systems. The addition of mass changes the mechanical impedance of the concrete specimen induced by damage. This procedure has the advantage of not causing permanent damage in the investigated concrete beam specimen. The overall possible damage and guided wave conditions can be summarized as:

Case NDNG : No damage – No Guided wave

Case NDYG : No damage – with Guided wave

Case YDNG : damage M1 – No Guided wave

Case YDYG : damage M1 – with Guided wave

Case 2YDNGa : damage M1+M2 – No Guided wave

Case 2YDYG : damage M1+M2 – with Guided wave

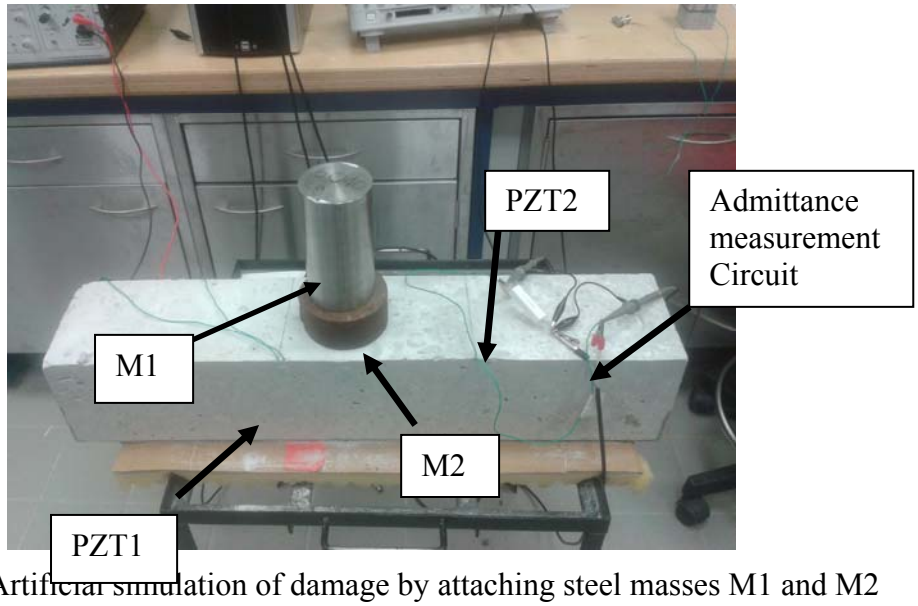

Figure 6: Artificial simulation of damage by attaching steel masses M1 and M2

Typical EMA FFT spectrums generated at the PZT2 surface for the simulated cases NDNG and YDNG conditions are depicted in Figure 7a and 7b. By observing those Figures, the effect of the damage M1 at the PZT2 admittance spectrum is not so clearly visible when there is no any guided wave activated from PZT1. This means that the distance of 100 mm is located away from the sensing area of PZT2 degrading the capability of EMA measurement in the detection of damage.

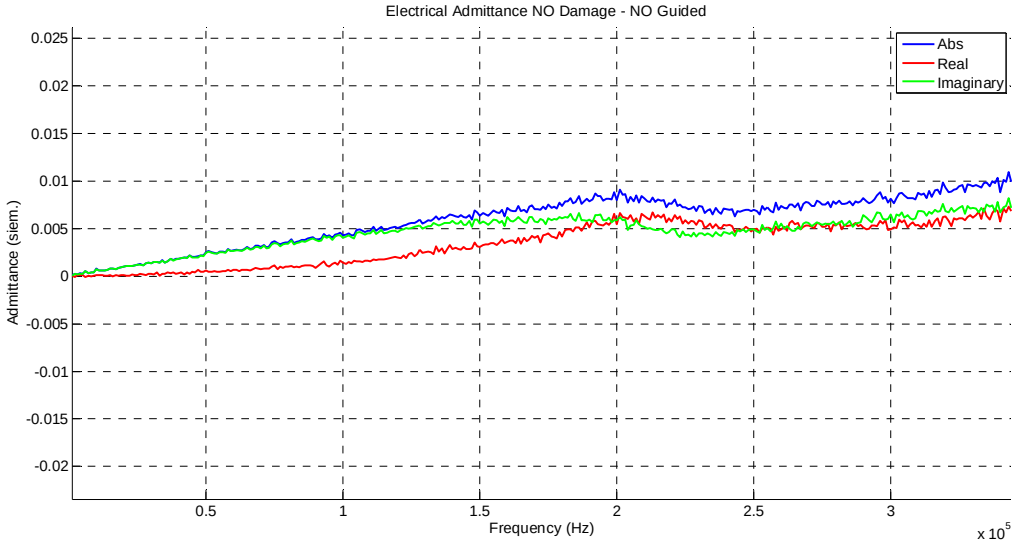

Figure 7a: FFT Admittance magnitude, real and imaginary part spectrums for NDNG case

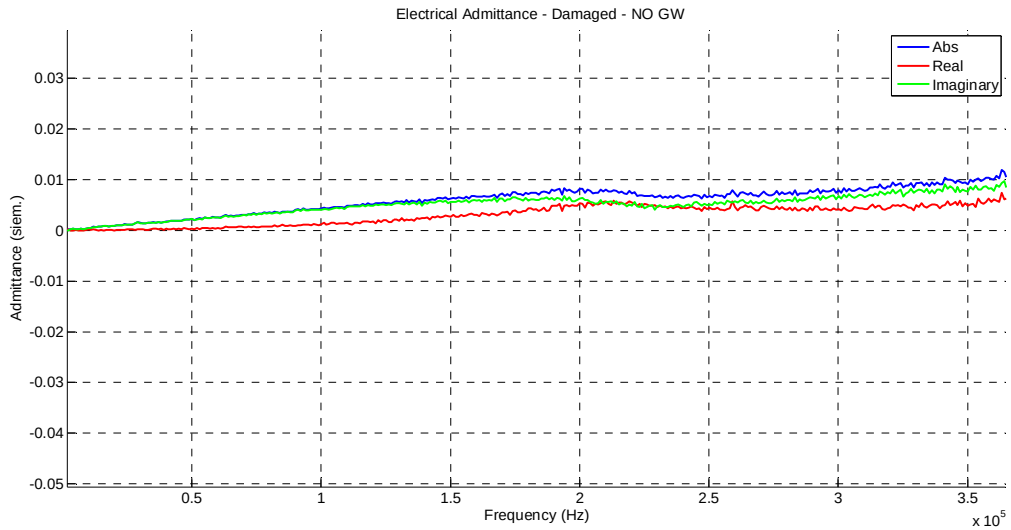

Figure 7b: FFT Admittance magnitude, real and imaginary part spectrums for YDNG case

Figure 8a and 8b present the EMA spectrums for the NDYG and YDYG cases. Although the differences between the two spectrum are also not so clearly visible but it is very interesting that comparing NDNG-YDNG and NDYG-YDYG figures the differences in spectrums NDYG-YDYG are more pronounced that those observing in NDNG-YDNG cases. This means that the introduction of guided wave enhance the sensing capabilities of EMA technique.

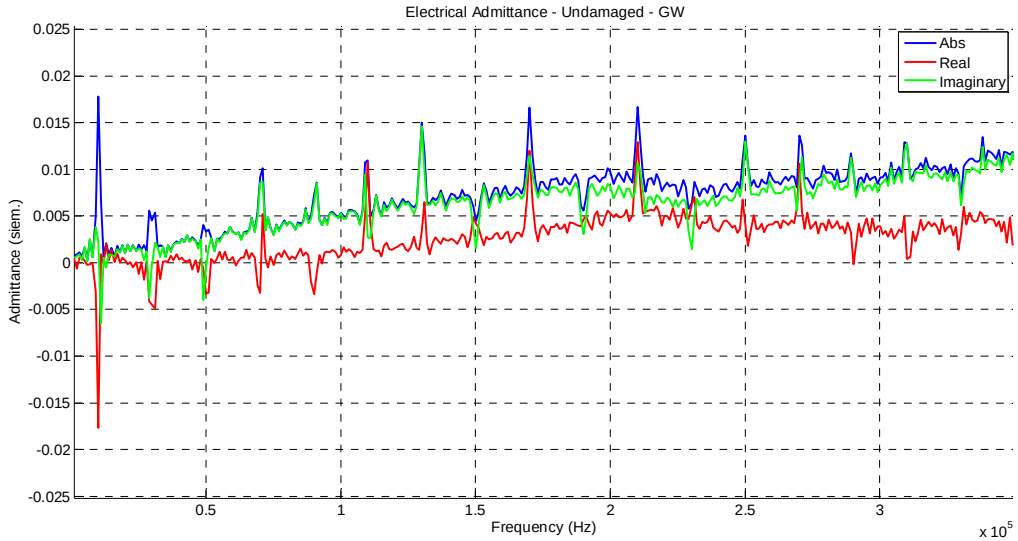

Figure 8a: FFT Admittance magnitude, real and imaginary part spectrums for NDYG case

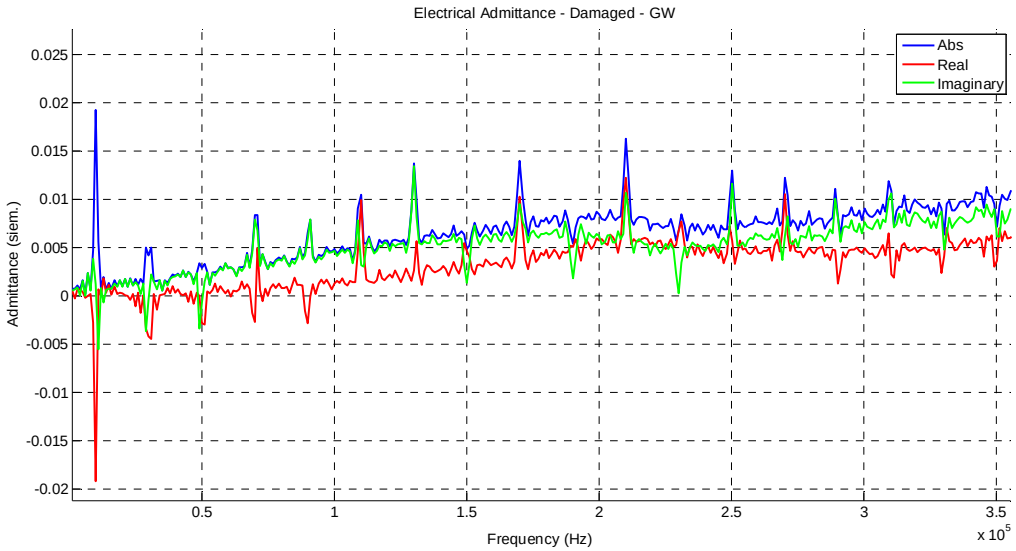

Figure 8b: FFT Admittance magnitude, real and imaginary part spectrums for YDYG case

By inspecting Figures 9a and 9b one can conclude that, since comparing those two figures the observed differences continues to be not so clear visible, the EMA spectrum as obtained by adding the second mass M2 do not provide more information for detecting this extended damage case when there is no any guided wave excitation. This means that although we added more damage in the system the EMA technique by itself is not so sensitive for damage located in a distance 100 mm away from sensing system.

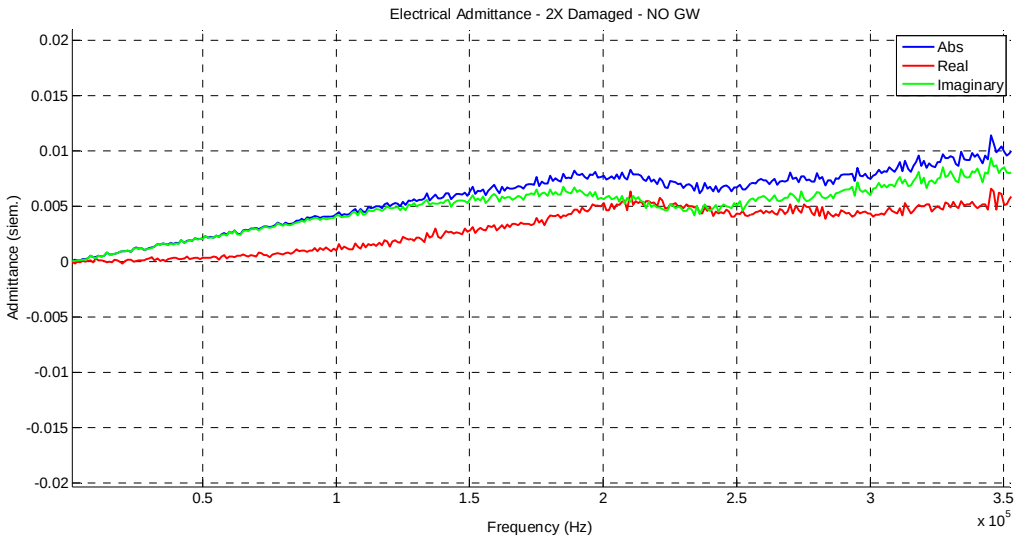

Figure 9a: FFT Admittance magnitude, real and imaginary part spectrums for 2YDNGa case

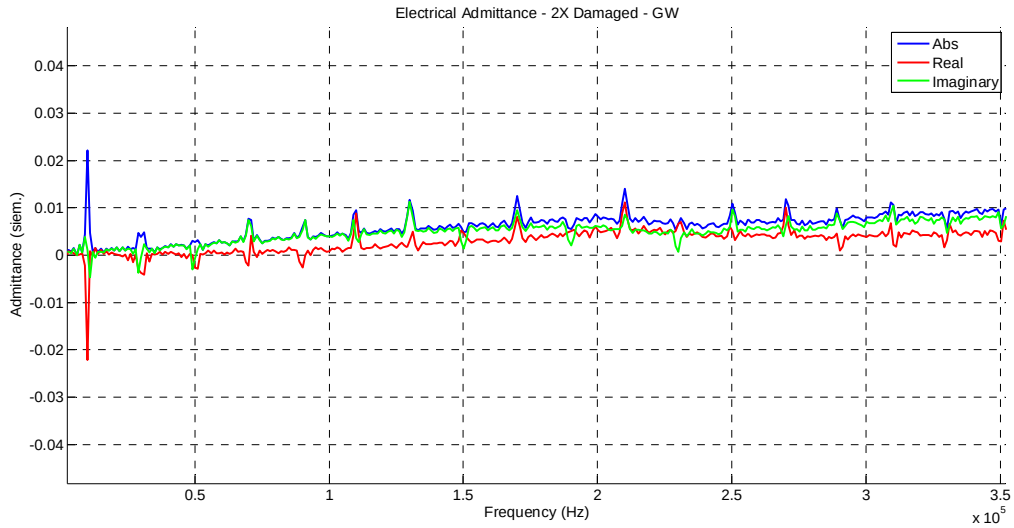

Figure 9b: FFT Admittance magnitude, real and imaginary part spectrums for 2YDYG case

Figure 10 displays the RMSD index variations of the absolute value of admittance spectrum as calculated under the investigated damage conditions. Thus, by observing this figure one may conclude that : a) RMSD index remains almost constant (0.0038 or 0.0036) when there is no any guided wave excitation, and b) RMSD increases from 0.0071 to 0.0107 values by just introducing the guided wave.

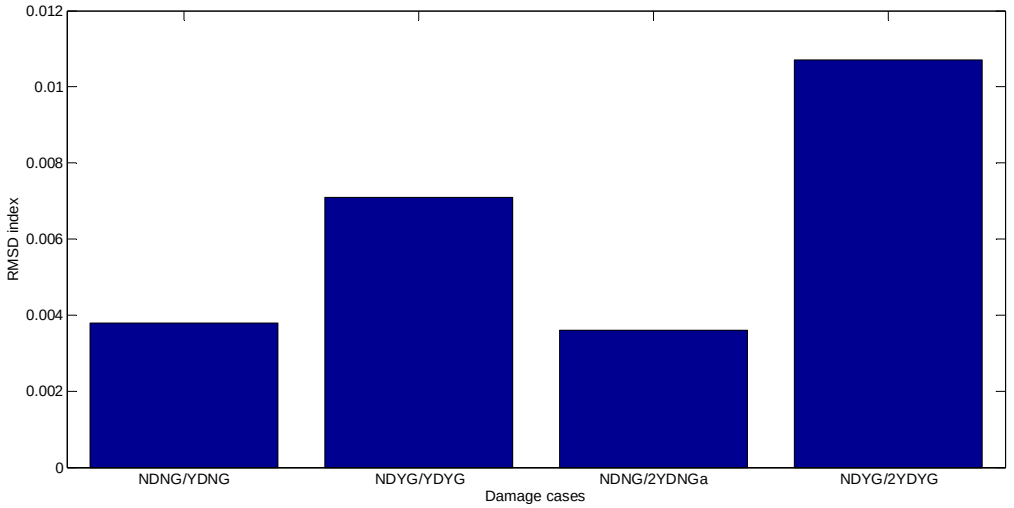

Figure 10: RMSD index as a function of damage cases

6 CONCLUSIONS

This paper presents a new method for SHM systems based on the combined utilization of impedance-based technique and guided-wave technique. The feasibility of the proposed technique has been investigated by finite element analyses and laboratory experiments. The proposed integrated system was able to successfully correlate both impedance and guided wave signals while in the same time its performance depends on the specific characteristics of its components. The results demonstrated that the simultaneous combination of those measuring techniques gives the benefit of simultaneous near and far-field damage detection in concrete structures.

ACKNOWLEDGEMENTS

This research has been co-financed by the European Union (European Social Fund – ESF) and Greek National Funds through the Operational Programme "Education and Lifelong Learning. Investing in Knowledge Society" of the National Strategic Reference Framework (NSRF 2007-2013) of the Ministry of Education & Religius Affairs, Culture &Sports-Research Funding Programme: THALIS.

REFERENCES

[1] Doherty, J.E. *Handbook of Experimental Mechanics,* Chapt.12, Society for experimental Mechanics,Inc, Bethel, CT, USA, 1987.
[2] Park, G., Cudney, H.H., and Inman, D.J. Impedance-based health monitoring of civil structural components. *Infrastuctures Systems* 6, 153-160.2,2000.
[3] Park, G., Cudney, H.H., and Inman, D.J. Overview of piezoelectric impedance-based health monitoring and pth forward. *The Shock and Vibration Digest* 35, 451-463.3, 2000.
[4] Doebling, S.W., Farrar, C.R., and Prime, M.B. A summary review of vibration-based damage identification methods. *The Shock and Vibration Digest* 30, 91-105, 1998.
[5] Song, G, Gu, H. and Mo Y-L. Smart aggregates: multifunctional sensors for concrete structures-a tutorial and a review*, Smart Mater Struct*., 17, 2008.
[6] Song G., Gu H., Mo YL, Hsu T and Dhonde H. Concrete structural health monitoring using embedded piezoceramic transducers, *Smart Mater. Struct.,* 16, 959-968, 2007.
[7] V. Georgiutiu, A. Zagrai, JJ Bao. Damage identification in aging arcraft structures with piezoelectric wafer active sensors. *Journal of Intelligent Materialsm Systems and Strucures*.
[8] Wai, JR, Park, G. Farrar, CR. Integrated structural health monitoring assessment using piezoelectric acticve senors. *Shock and Vibration*, 12(6), 389-405, 2005.
[9] S.W Zhou, C.A. Liang, C.A. Rogers. Integration and Design of Piezoceramic Elements in Intelligent Structures. *Journal of Intelligent Materials Systems and Structures* 6, 733-743,1995.
[10] Liang, C., Sun, F.P. and Rogers, C.A. Coupled Electro-mechanical Analysis of Adaptive Material Systems Determination of the Actuator Power Consumption and System Energy Transfer. *Journal of Intelligent Materials Systems and Structures*, 5, 15-20, 1994.

[11] Bhalla, S. and Soh, C.K. High Frequency Piezoelectric Signatures for Diagnosis of Seismic Blast Induced Structural Damages. *NDT and E. Int*. 37,23-33, 2004.
[12] QuadTech Inc, USA, www.quadtechworld.com
[13] Cypher Instruments Ltd, www.cypherinstruments.co.uk
[14] Agilent Application Note 1405-2: Dynamic Signal Analysis, Agilent Technologies Ltd
[15] National Instruments, USA, www.ni.com
[16] A.A Lab Systems Ltd, Israel, www.labsystems.com